Applied Thermal Engineering 76 (2015) 64–75

Contents lists available at ScienceDirect

Applied Thermal Engineering

journal homepage: www.elsevier.com/locate/apthermeng

Research paper

Effects of furnace chamber shape on the MILD combustion of natural gas

Yaojie Tu, Hao Liu*, Sheng Chen, Zhaohui Liu, Haibo Zhao, Chuguang Zheng

State Key Laboratory of Coal Combustion, Huazhong University of Science and Technology, Wuhan 430074, PR China

HIGHLIGHTS

- The impact of furnace body configuration on MILD combustion was studied.
- Stronger recirculation and smaller temperature gradient are achieved at larger divergence angle.
- Larger backflow and chemical flame occupations are obtained at larger divergence angle.
- NO emission reduces at larger divergence angle.
- Larger divergence angle is helpful for establishing MILD combustion.

ARTICLE INFO

Article history:
Received 21 July 2014
Accepted 5 November 2014
Available online 13 November 2014

Keywords:
MILD combustion
Furnace chamber shape
Numerical simulation
NO_x emission

ABSTRACT

The objective of this work is to assess the effects of furnace chamber shape (by changing the angle α between the furnace roof and sidewall) on the MILD (moderate or intense low-oxygen dilution) combustion characteristics for natural gas using high temperature air (1573 K) with the aid of CFD simulations. The present simulations agree well with the previous experimental results, and some new findings are revealed. For instance, when increasing angle α under the present furnace-burner conditions, stronger recirculation, smaller temperature gradient as well as larger reaction zone are obtained, indicating the easier establishment of MILD combustion. In contrast, the combustion regime transforms from MILD combustion towards flame combustion in the stability limits of diffusion combustion provided by Wünning et al. (Prog. Energy Combust. Sci. 23 (1997) 81–94) when reducing angle α. It is also suggested that there is a critical value for angle α below which MILD combustion cannot be established under the present conditions.

© 2014 Elsevier Ltd. All rights reserved.

1. Introduction

Moderate or intense low-oxygen dilution (MILD) combustion [1] has become one of the most promising combustion technologies in industrial heating for low NO_x emission and high efficiency of combustion. MILD combustion is featured as intense recirculation of hot flue gas inside the furnace, which on one hand improves the temperature of reactants above their ignition point, on the other hand dilutes the mixture of reactants before combustion. In this regard, combustion takes place in an environment of highly diluted reactants where auto-ignition is also allowed to happen. The combustion process under MILD condition is very different from conventional combustion since the internal recirculation is so strong that the combustion reaction zone spreads to a broader space. Hence, both the temperature and the chemical species are distributed homogeneously, and the peak temperature as well as NO_x emission is reduced as well.

This technology is also named as high temperature air combustion (HiTAC) when highly preheated temperature air is used (usually >1000 °C) [2,3], or flameless combustion or flameless oxidation (FLOX) [4,5], or colorless distributed combustion (CDC) [6,7]. For convenient description, the term “MILD combustion” is used uniformly throughout the present paper. Plenty of valuable work has been done on MILD combustion by such as Cavaliere et al. [1], Tsuji et al. [2,3], Wunning et al. [4,5], Gupta et al. [6,7], Webber et al. [8–13], Blasiak et al. [14–16], Dally et al. [17,18] and Mi et al. [19–23] Moreover, detailed descriptions for MILD combustion and HiTAC have been respectively reviewed by Cavaliere et al. [1] and Tsuji et al. [3] To summarize, Wünning et al. gave the major clarifications of MILD combustion in ref [5], and demonstrated that the

* Corresponding author.
E-mail addresses: liuhao@hust.edu.cn, liuhao@mail.hust.edu.cn (H. Liu).

http://dx.doi.org/10.1016/j.applthermaleng.2014.11.007
1359-4311/© 2014 Elsevier Ltd. All rights reserved.

Nomenclature

α	angle between furnace roof and sidewall
τ_{ch}	characteristic time scale of chemical reaction
τ_{turb}	characteristic time scale of turbulent mixing
Y_i	mass fraction of species (i)
$\vec{v}$	velocity vector
$\overrightarrow{J_i}$	mass diffusion flux of species (i)
R_i	net production rate of species (i)
V_x	x component of mean velocity
K_V	internal recirculation rate
ρ	mixture density
A_r	reference furnace cross sectional area
A_a	absolute furnace cross sectional area
m_e	entrained flue gas mass flow rate
m_f	fuel mass flow rate
m_a	air mass flow rate
K_v^*	equivalent internal recirculation rate
R_O	oxidation mixture ratio
m_O	local oxygen mass fraction
m'_O	oxygen mass fraction needed to complete combustion
R_C	critical oxidation mixture ratio
R_F	chemical flame occupation degree

realization of MILD combustion has nothing to do with operational conditions like fuel types, air or fuel preheating temperature, nor burner or furnace configurations, as long as there exits an intense recirculation of hot combustion products inside the furnace. So far, MILD combustion has been applied in the industrial furnaces, especially in steel making. However, R&D of MILD combustion mainly deals with gaseous fuels and light oils due to their preferable combustion characteristics to solid fuels, but the latest studies of MILD combustion with solid fuels like pulverized coal and biomass still can be found elsewhere [8,11–13,16,18,24–36].

It is worth mentioning that the IFRF (International Flame Research Foundation) [8–12] has carried out a series of MILD combustion experiments for natural gas, light oil, heavy oil and pulverized coal with high temperature air, which leads to a deep insight into the fundamental and practical issues of MILD combustion. All the tests by IFRF were conducted on a 0.58 MW vertical furnace with the burner inlets and the exhaust gas exit located at the opposite side of the furnace walls. Later, a series of MILD combustion experiments with natural gas, sawdust and pulverized coal under both O_2/N_2 and O_2/CO_2 atmospheres were carried out at Adelaide [17,18] on a 20 KW recuperative furnace with the burner inlets and the exhaust gas exit located at the same side of the furnace walls. According to the experimental and simulation results of the above two furnaces which have different geometrical configurations, the internal recirculation is usually found to be stronger inside the Adelaide's furnace as compared to the IFRF's furnace. The reason behind this is that for Adelaide's furnace, the combustion products would totally flow back into the upstream furnace; while

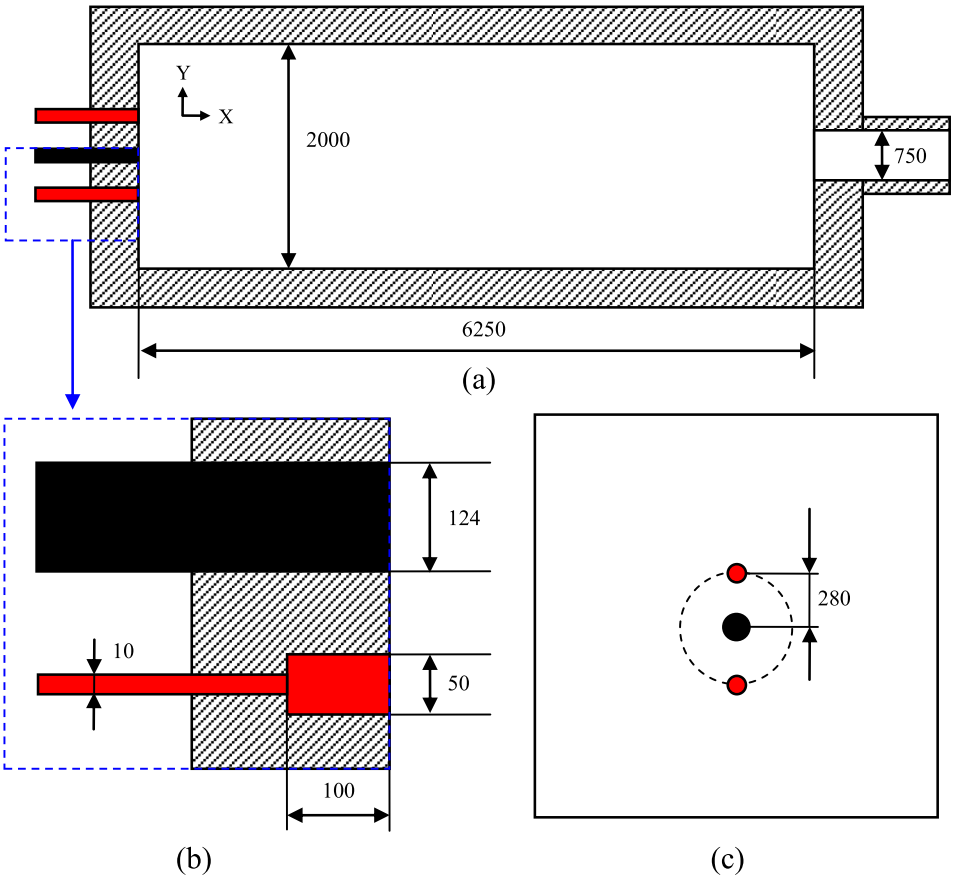

Fig. 1. Schematic diagram of the reference furnace-burner system: (a) the furnace; (b) the burner; (c) top view of the furnace (unit: mm).

Table 1
Experimental conditions in IFRF test [9].

	Flow rate (kg/h)	Temperature (K)	Enthalpy (MW)	Components (vol.%)
Fuel	47	298	0.58	$CH_4 = 87.8$, $C_2H_6 = 4.6$, $C_3H_8 = 1.6$, $N_2 = 5.5$
Oxidizer	830	1573	0.35	$O_2 = 19.5$, $N_2 = 59.1$, $H_2O = 15$, $CO_2 = 6.4$, NO = 110 ppm
Exhaust gases	877	1493	0.38	$O_2 = 1.6$, NO = 140 ppm

Table 2
Furnace geometrical parameters of the considered cases.

	Case1	Case2	Case3	Case4	Case5
α	80°	85°	90°	95°	100°
L_1 (mm)	2998	2524	2000	1426	795
L_2 (mm)	795	1426	2000	2524	2998

for IFRF's furnace, only part of the combustion products recedes backward. This to some extent indicates that the internal configuration of furnace or its exit location can be an important factor on the internal dynamic flow field, but not only the burner system.

Over the recent years, the investigations on MILD combustion which were related to the geometrical parameters mainly focused on the burner system [17–22,35–38] (e.g. injection velocity or direction, nozzle separation distance, mixing pattern, burner location and arrangement). Both the experiments and numerical simulations were carried out to study the above parameters. However, less work has been done with the furnace internal configuration, namely the combustion chamber shape. On this side, Schaffel N. et al. [13] proposed a conceptual design of a supercritical boiler utilizing MILD combustion technology, and they found that the varied boiler body shapes made a difference to the internal recirculation, coal burnout ratio as well as the temperature distribution (which is a dominant factor on thermal NO_x formation). By properly designing the boiler parameters, higher combustion efficiency and heat flux as well as lower NO_x emission could be realizable under MILD combustion in comparison with conventional boiler. In this regard, the geometrical parameters of the burner as well as the combustion chamber itself can play very important role on the furnace internal recirculation, which is the essential condition for achieving MILD combustion.

From the academic point of view, flame structure can be influenced or even dominated by the dynamic flow inside the furnace. However, the internal dynamic flow is significantly depended on the characteristics of both burner and combustion chamber configurations. Up to now, there are kinds of burners designed for ordinary or specific applications, i.e. direct flow burner, swirl burner, staged burner, and MILD burner. The different design concepts of the burners rely on the different demands, for example, swirl burner is featured as central recirculation of hot flue gas to enhance the ignition stability, while MILD burner is applied to obtain a uniform temperature field and lower NO_x emission. As for furnace chamber configuration, normal patterns of cylinder or cubic shapes are mostly used for researches. The regime from conventional combustion to MILD combustion is transformed by simply replacing the corresponding burners. However, the potential impact of furnace chamber shape on combustion characteristics is barely studied, especially under MILD operation. On the other hand, reheating furnace is one of the top energy consuming industrial devices, thus it is necessary to optimize the geometric parameters to obtain better performance and save energy, especially when the function of a furnace changes or new furnace is going to be built.

The main objective of the present study is to investigate the effects of furnace chamber shape (by changing the angle α between the furnace roof and sidewall) on MILD combustion with the aid of CFD simulation based on the IFRF experimental instrument. First, experimental data from the reference case ($\alpha = 90°$) was employed to validate the present simulations. Then, the characteristics of internal mixing, combustion as well as NO_x emission were respectively compared for the considered cases. This study has figured out the change rules of the in-furnace flow fields and combustion behaviors against the angle α, and can provide some useful information on optimizing furnace geometric parameters under MILD operation.

2. Computational details

2.1. Reference conditions and considered furnace shape

The MILD combustion experiment with natural gas of the reference case were performed by IFRF in a semi-industrial scale furnace (see Fig. 1) with a 2 m × 2 m cross section and a length of 6.25 m [9,10]. The burner system was consisted of a central oxidizer nozzle and two off-axis fuel nozzles. The internal diameter of the oxidizer and fuel nozzles were 124 mm and 10 mm, respectively. The distance between the oxidizer and fuel nozzles was 280 mm. The furnace was operated at 0.58 MW fuel input with the oxidizer preheated to 1573 K. Table 1 lists the experimental conditions of the IFRF test. Note that, the high temperature oxidizer was generated from a pre-combustor, therefore, a small quantity of H_2O and CO_2

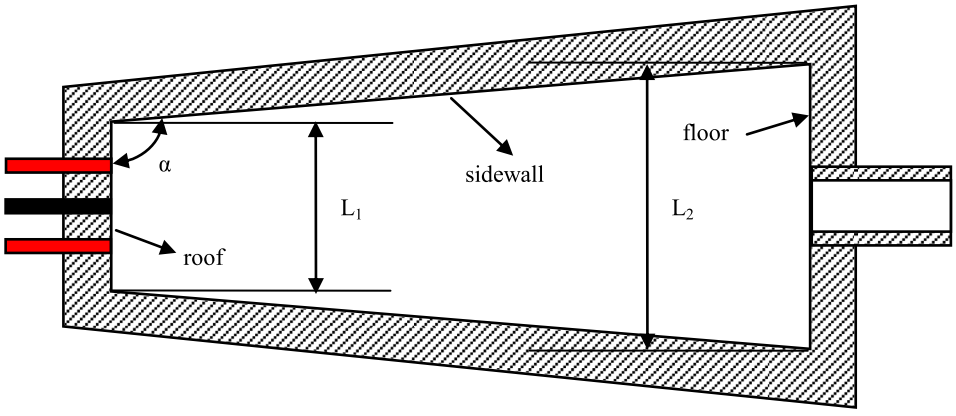

Fig. 2. Schematic diagram of the considered furnace chamber shape.

Table 3
Global reaction mechanism of NG used in the present study (units in SI).[a]

Index	Reactions	A [kmol/(m^3 s^{-1})]	Ea (J/kmol)	Reaction orders
R.1	$CH_4 + 0.5O_2 \rightarrow CO + 2H_2$	4.4×10^{11}	1.255×10^8	$[CH_4]^{0.7}[O_2]^{0.8}$
R.2	$CO + 0.5O_2 \rightarrow CO_2$	2.24×10^{12}	1.703×10^8	$[CO][O_2]^{0.25}[H_2O]^{0.5}$
R.3	$H_2 + 0.5O_2 \rightarrow H_2O$	5.69×10^{11}	1.46×10^8	$[H_2][O_2][H_2O]$
R.4	$C_2H_6 + 3.5O_2 \rightarrow 2CO_2 + 3H_2O$	6.186×10^9	1.256×10^8	$[C_2H_6]^{0.1}[O_2]^{1.65}$
R.5	$C_3H_8 + 5O_2 \rightarrow 3CO_2 + 4H_2O$	6.186×10^9	1.256×10^8	$[C_3H_8]^{0.1}[O_2]^{1.65}$

[a] The reaction rate coefficient $k = A\exp(-E_a/R_uT)$, where $R_u = 8315$ J kmol^{-1} K^{-1}.

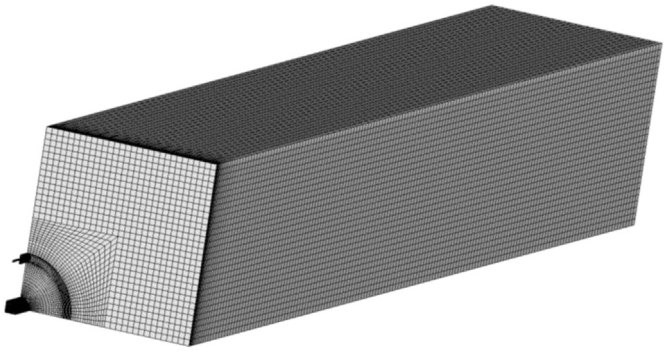

Fig. 3. Computational grid for simulating the reference case with 565224 cells.

were contained in the oxidizer together with a relatively large quantity of NO.

The considered furnace chamber shapes in the current study were varied by changing the angle α between the furnace roof and sidewall as illustrated in Fig. 2. Five angles were examined including two acute angles ($\alpha = 80°$, and $\alpha = 85°$), a right angle ($\alpha = 90°$, the reference case), and two obtuse angles ($\alpha = 95°$, and $\alpha = 100°$). Note that, the total length and the volume of the furnace were kept unchanged in order to have a same average volume heat load as well as residence time. The side length of the furnace roof and floor were summarized in Table 2 together with the corresponding angle.

2.2. Simulation approaches

The simulations were performed with the aid of the commercial CFD (computational fluid dynamics) software ANSYS Fluent 14.0. The viscous turbulent flow was solved using standard κ-ε model and standard wall function [39]. The P1 model with the weighted sum of gray gas model (WSGGM-domain-based) was used to solve the radiation and absorption between the gaseous molecules and furnace walls [24,40]. The SIMPLE scheme was used for pressure–velocity coupling [41]. The main challenge in simulating MILD combustion is to select a proper combustion model. Since the mean reaction rate under MILD condition is slower than conventional combustion, the characteristic time scale of chemical reaction (τ_{ch}) becomes comparable to that of turbulent mixing (τ_{turb}), thus the turbulence–chemistry interactions should be treated with finite rate approaches [42]. In this regard, the eddy-dissipation model (EDM) and the eddy-dissipation concept (EDC) are expected to be considered in modeling MILD combustion. However, in the present CFD codes, the EDM allows only a two-step global mechanism, while the EDC allows both global and detailed mechanisms. Moreover, M. Vascellari et al. [24] have demonstrated that the

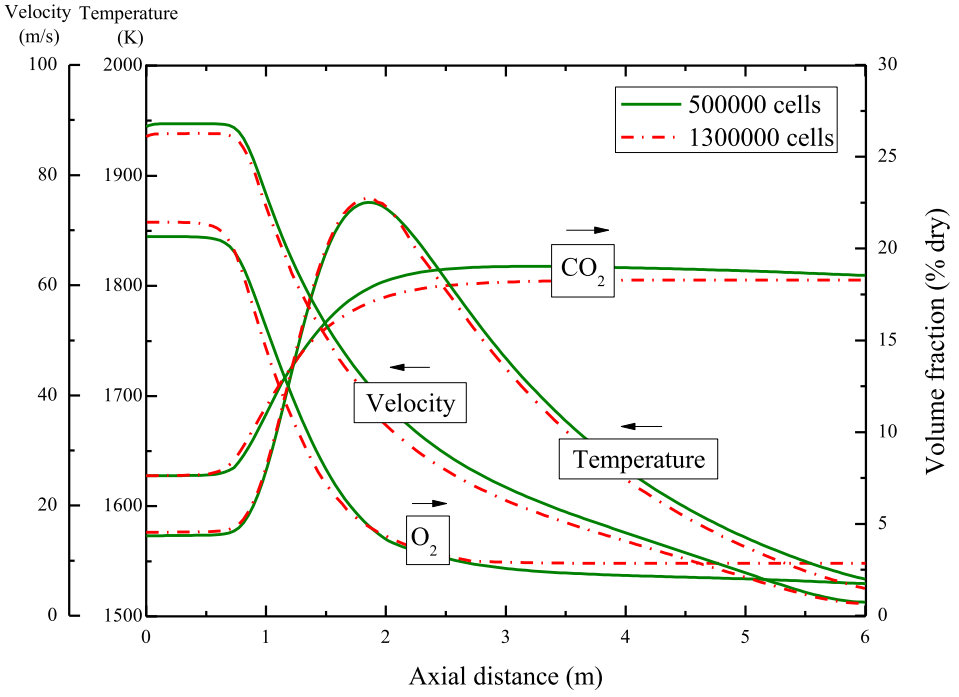

Fig. 4. Grid-independence test in axial temperature, velocity, O_2 and CO_2 distributions for the reference case.

coupling of EDC with detailed mechanism would produce better results of the MILD combustion. Therefore, we choose EDC as the combustion model in the present study rather than EDM.

In the EDC model, the transporting equations for the chemical species are governed by:

$$\frac{\partial}{\partial t}(\rho Y_i) + \nabla\left(\rho \vec{v} Y_i\right) = -\nabla \cdot \overrightarrow{J_i} + R_i \tag{1}$$

where ρ is the mixture density, Y_i is the local mass fraction of each species (i), $\vec{v}$ is the velocity vector, and $\overrightarrow{J_i}$ is the mass diffusion flux of species (i), and R_i is the net rate of production of species (i) by chemical reaction. The mass diffusion flux $\overrightarrow{J_i}$ and the chemistry source term R_i of ith species are calculated by:

$$\overrightarrow{J_i} = -\left(\rho D_{i,m} + \frac{\mu_t}{Sc_t}\right)\nabla Y_i \tag{2}$$

$$R_i = \frac{\rho \xi^2}{\tau\left(1-\xi^3\right)}\left(Y_i^* - Y_i\right) \tag{3}$$

where Sc_t is the turbulence Schmidt number, $D_{i,m}$ is the mass diffusion coefficient for each species, ξ is the size of fine scales, and Y_i^* is the fine-scale species mass fraction after reacting.

In order to reduce the calculation consumption, a five-step global reaction mechanism is used in the present study for the fuel as listed in Table 3. The global mechanism contains three reactions for CH_4 and one reaction for C_2H_6 and C_3H_8, respectively. To examine the suitability of the global reaction mechanism on modeling MILD combustion, the simulations of the reference case with a detailed chemical kinetic mechanism for CH_4 from GRI-Mech 3.0 [43] is also carried out. As indicated by M. Vascellari et al. [24], the low NO_x concentration has a reduced impact on the other flow properties, like temperature and species distributions as well as mass, momentum and energy balances. Moreover, due to the longer characteristic time scale of NO_x kinetic with respect to the combustion kinetics, the NO_x production can be evaluated by post-processing approach [24]. Finally, the N-containing reactions are removed in GRI-Mech 3.0 mechanism, and only 219 reversible reactions with 36 chemical species are calculated.

The fuel, oxidizer and flue gas boundary conditions were set as constant mass flow inlet and pressure outlet, respectively. The furnace wall was set at constant temperature of 1500 K with a

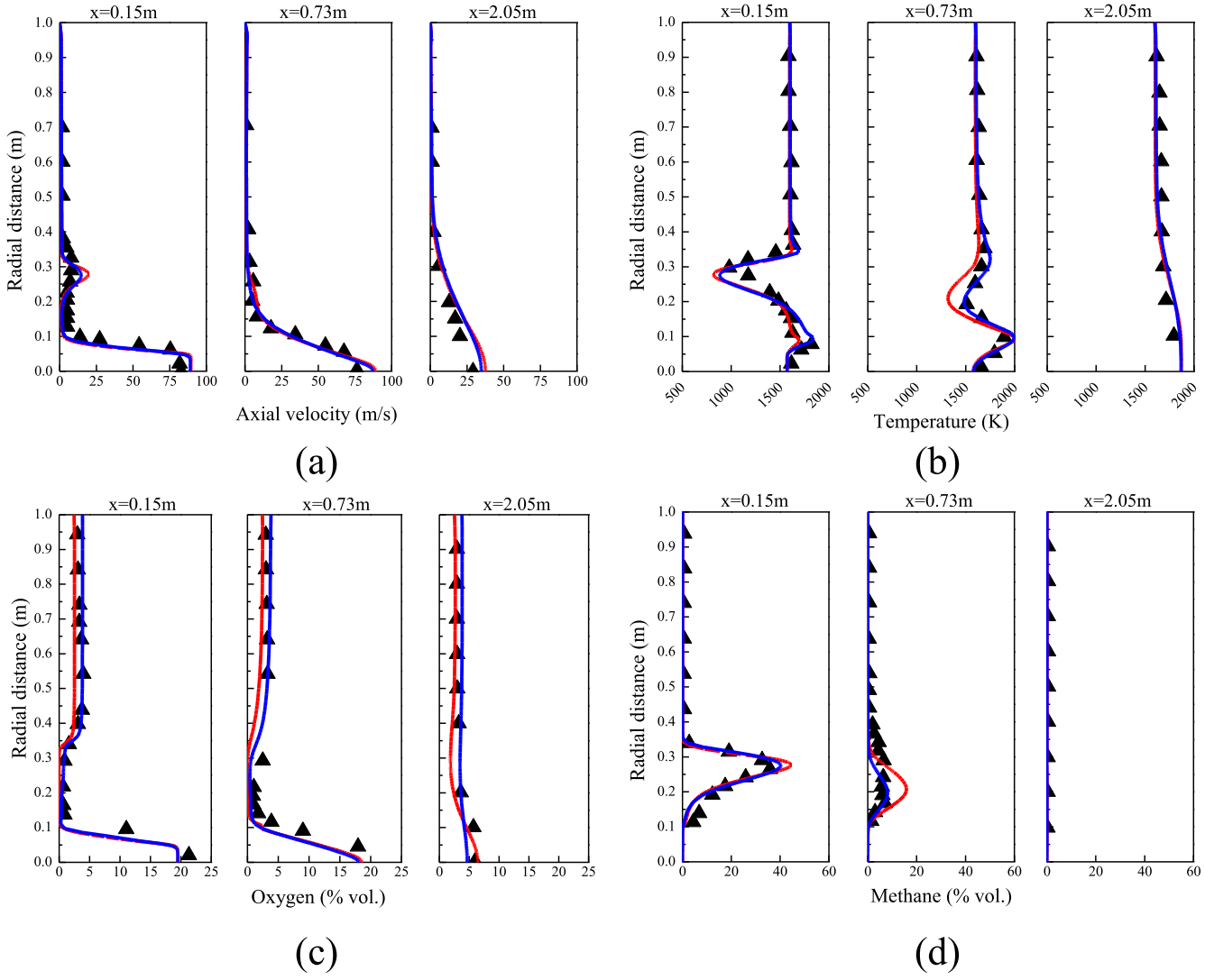

Fig. 5. Comparison of the experimental(▲) and simulated(—global mechanism, —GRI 3.0 mechanism) results of the reference case: (a) velocity; (b) temperature; (c) oxygen concentration; (d) methane concentration at x = 0.15 m, 0.73 m, 2.05 m, z = 0 m.

constant internal emissivity rate of 0.6. Convergence was obtained when the residence of continuity was lower than 10^{-5}, and 10^{-6} for the other variables (velocity, energy, P1 and species, etc.). In addition, the maximum temperature and velocity on the symmetrical plane ($z = 0$) was monitored, regarded as another criterion for convergence when their variations were less than 1 K and 0.1 m/s, respectively.

3. Results and discussion

3.1. Grid-independent test

Owning to the symmetrical geometry of the present furnace, only one quarter of the furnace was modeled. Fig. 3 shows the computational grid used for simulating the reference case, which is consisted of 565224 hexahedral cells with size functions on the furnace roof and sidewall. In order to check the independence of the grid, simulation work was also conducted for the reference case with a fine grid consisted of 1319902 cells. Refinement on the furnace roof and sidewall was made to the grid. Fig. 4 compares the gas temperature, velocity, O_2 and CO_2 distribution profiles along the furnace centerline from the two grids. As demonstrated, no obvious difference in the axial temperature, velocity and species distributions can be distinguished between the coarse grid and the fine grid. In order to save the computational time, the coarse grid with 565224 cells was utilized for simulating the reference case, and similar meshing method and grid size were employed for the subsequent cases.

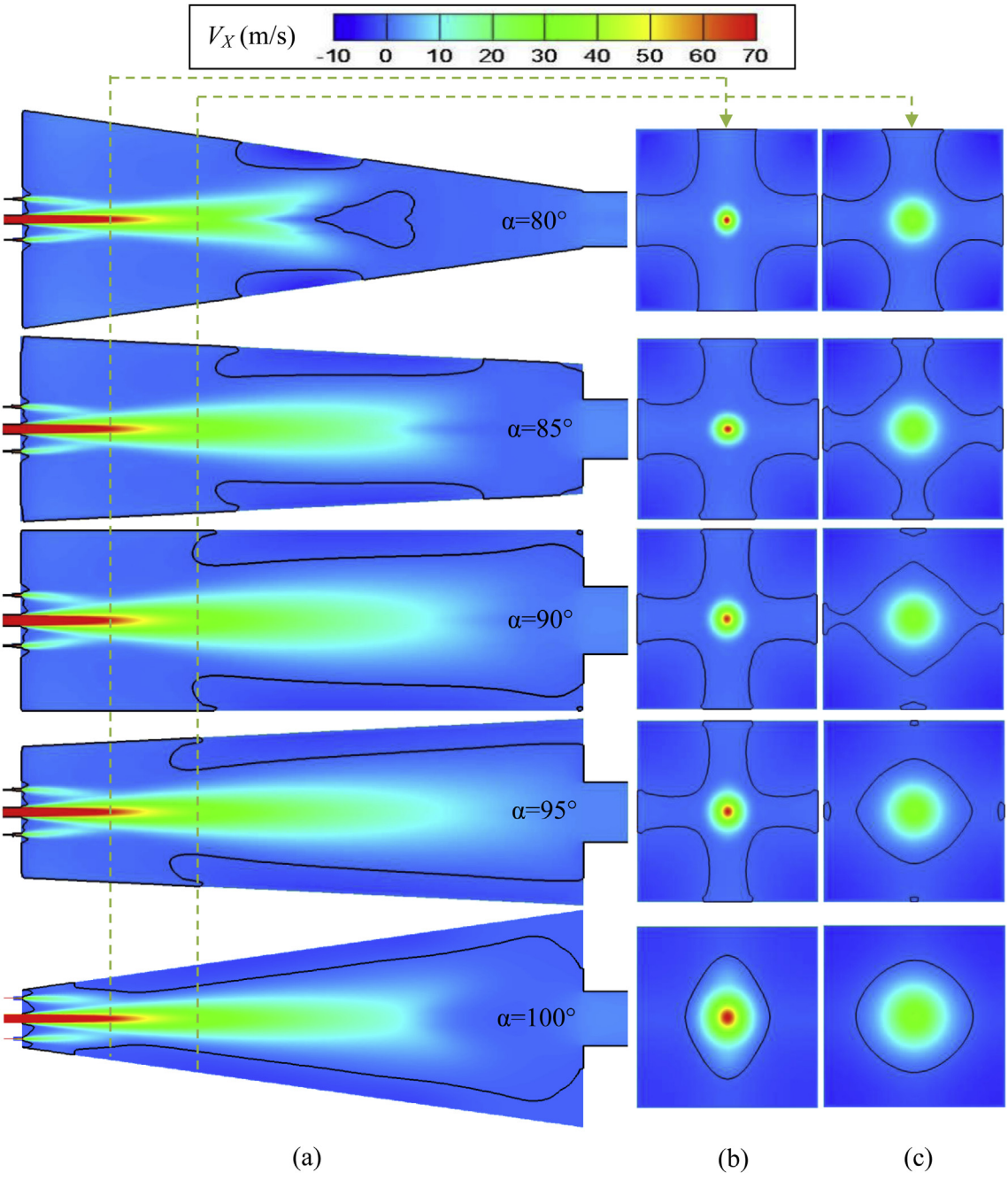

Fig. 6. Contours of x component of mean velocity (a): x-y plane ($z = 0$); (b): $x = 1000$ mm plane; (c): $x = 2000$ mm plane. The black curves denote the level of $V_x = 0$.

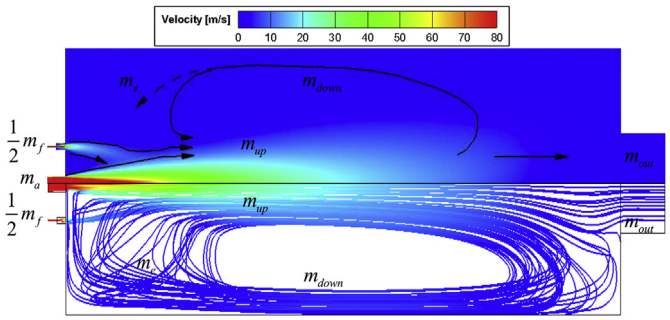

Fig. 7. Schematic diagram of the velocity field (up) and aerodynamic flow field (down) inside the furnace for the reference case.

3.2. Validation of the computational models

In order to examine the adequacy of the adopted models with the global reaction mechanism in the present study, numerical simulations were also carried out using the detailed mechanism from GRI-Mech 3.0 for the reference case. The simulated results of mean velocity, temperature, O_2 and CH_4 concentrations in furnace from both global and detailed mechanisms were compared with the experimental data [9,10] at different measurement locations (see Panels a–d of Fig. 5).

As displayed in Fig. 5, the calculated results from both global and detailed mechanisms have shown good agreement with the measured data for all of the above parameters. However, the simulated results of temperature and CH_4 concentration distributions from the global mechanism seem to be unsatisfactory near the fuel injection zone ($Y = 280$ mm). In addition, the O_2 consumption is found to be improved with the global mechanism. The reason behind these differences is probably that, the simplified global mechanism has not taken the intermediate species (i.e. CH, OH, etc.) into account, and local details of the chemical reaction cannot be precisely captured especially in the fuel rich region. Nevertheless, the characteristics of the dynamic flow field and combustion status still can be generally expressed with the global mechanism. Since the computing cost increases remarkably with the GRI-Mech 3.0 mechanism, the simplified global mechanism is adopted to save the computing consumption.

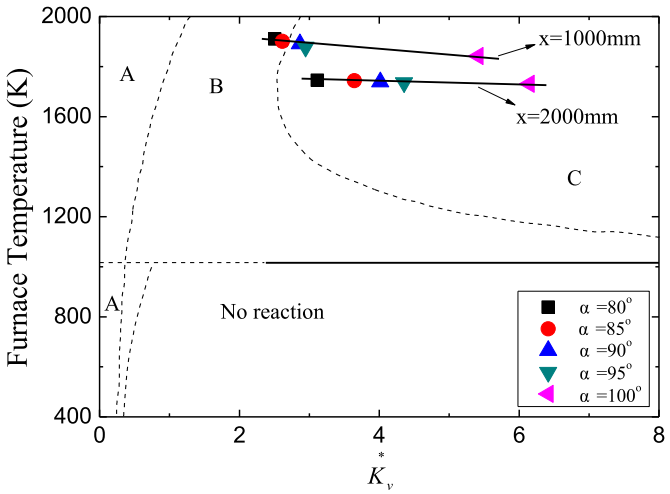

Fig. 8. Furnace temperature against K_v^* for the present simulation cases and the schematic diagram of stability limits for methane in diffusion combustion from Ref. [4].

3.3. Effects of furnace chamber shape on mixing

MILD combustion is characterized as intense recirculation of flue gas inside the furnace, and Fig. 6 shows the contours of the x component of mean velocity (V_x) in the x-y plane ($z = 0$) and the y-z planes at $x = 1000$ mm and 2000 mm for the five cases. The border ($V_x = 0$) between the upward and downward velocity can be distinguished by the black curves and the contour legend. Similar flow field distributions can be observed for the five cases. Concretely, they all have a central upward flow ($V_x > 0$) and downward backflows ($V_x < 0$) near the furnace sidewalls and four corners. Note that, the backflow even can be observed in the furnace central region when $\alpha = 80°$. As observed, with an increase of angle α, the position where backflow starts occurring in x-y plane ($z = 0$) is moving towards upstream furnace. Meanwhile, the occupation of backflow in x-y plane is becoming larger as angle α increases. Especially when $\alpha = 100°$, the backflow occupies the whole surrounding area of the central upward flow throughout almost the whole furnace.

Fig. 7 illustrates the simplified schematic diagram of the in-furnace flow and aerodynamic fields. In order to identify the dilution degree of reactants by entrained flue gas, here, the internal recirculation rate K_V is introduced, which is first defined by Wünning et al. [4] as the ratio of mass flow rate of the entrained flue gas (m_e) to that of the initial fuel (m_f) and air (m_a) jets at a certain plane (see Fig. 7). It is expressed as:

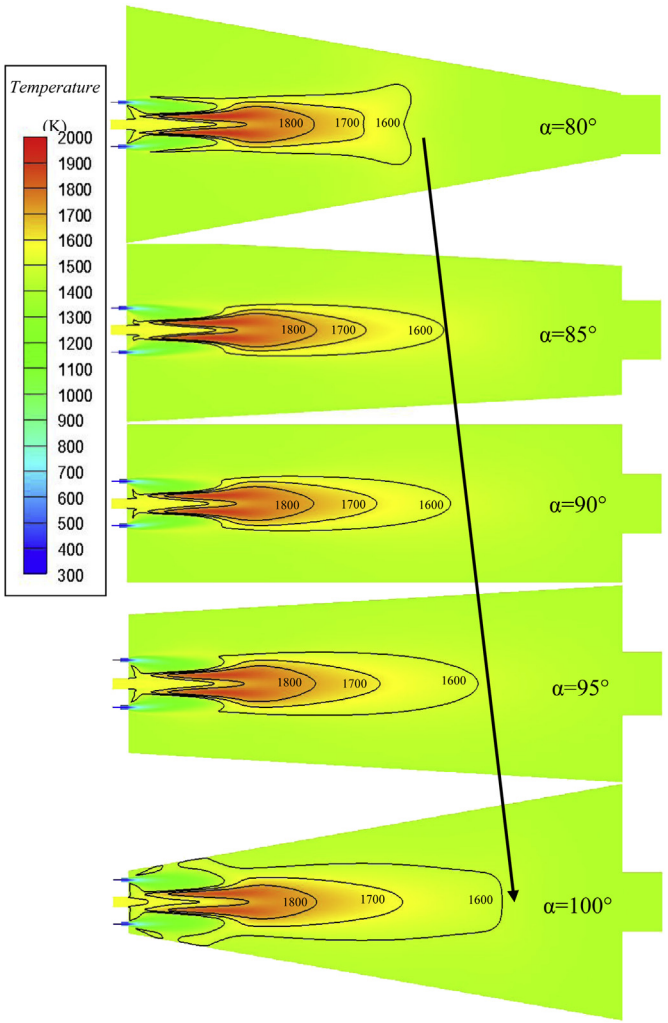

Fig. 9. Contours of temperature fields in the x-y plane ($z = 0$) for the five cases.

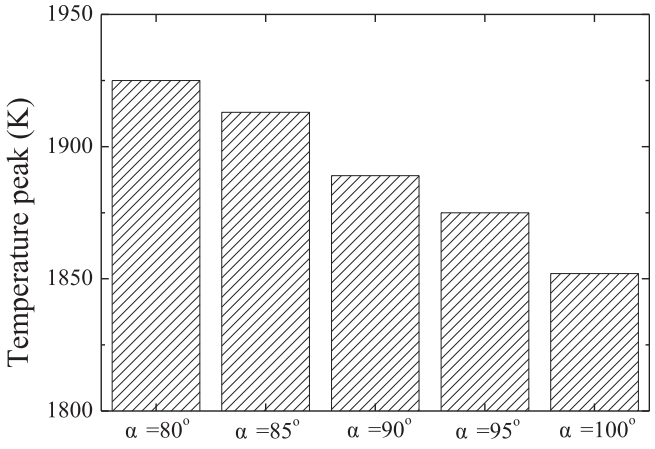

Fig. 10. Temperature peak for the five cases.

$$K_v = \frac{m_e}{(m_a + m_f)} = \frac{m_{up} - m_a - m_f}{(m_a + m_f)} = \frac{\iint_{A(up)} \rho v_x dydz - m_a - m_f}{(m_a + m_f)} \quad (4)$$

where $A(up)$ is the total area in a certain cross section with an upward axial velocity (v_x>0), and is represented by the central part within the black curves as shown in Fig. 6b–c. Note that, the cross sectional area at a fixed axial distance varies with different angle α, particularly, in the upstream furnace (x < 3125 mm), the cross sectional area reduces as angle α increases. To eliminate this geometrical discrepancy, the equivalent internal recirculation rate $\overset{*}{K}_v$ is used here, and is expressed as:

$$\overset{*}{K}_v = \frac{A_r}{A_a} K_v \quad (5)$$

where A_a is the absolute cross sectional area at a certain axial distance, and A_r is the reference cross sectional area at the same axial distance. In the present study, case3 is the reference case with a constant cross sectional shape along the furnace centerline. Thus, $A_r = 1m^2$ (one quarter of the geometry is simulated) is used for the $\overset{*}{K}_v$ calculations.

Fig. 8 shows the relationship between the K_V and the furnace temperature in diffusion combustion for methane, which was provided by Wünning et al. [4]. According to Fig. 8, the flame stability limit is consisted of three regimes (regions A, B, C stands for stable conventional combustion, unsteady transitional regime, MILD combustion). Since methane takes up the largest proportion (87.8% by volume) in the present fuel, the relationship in Fig. 8 could be applied in order to identify the combustion regime of the present cases regardless of slight difference in fuel composition. Therefore, the corresponding equivalent recirculation rate $\overset{*}{K}_v$ in x = 1000 mm and x = 2000 mm planes versus the furnace temperature for the five cases is also plotted in Fig. 8.

From Fig. 8, it can be found that the main reaction zone (see Fig. 12) is generally in the regime of MILD combustion for all of the five cases, except for case1 and 2 in x = 1000 mm plane. Hence, it is revealed that there exists a critical value for angle α below which the steady MILD combustion would not occur under the present conditions. Furthermore, it implies that when establishing MILD combustion in a furnace with a relatively small angle α, the initial injection conditions might need to be intensified (such as increasing injecting velocity or preheating), while in a furnace with a relatively large α, the initial injection condition could be relaxed, and it is also helpful for achieving MILD combustion.

In addition, the combustion regime movement against angle α is observed of a similar rule in both x = 1000 mm and x = 2000 mm planes according to Fig. 8. Specifically, the larger α always leads to lower temperature and improved $\overset{*}{K}_v$ at a certain cross section, this trend can be clearer when α = 100°. It indicates that increasing angle α can strengthen the mixing between the reactants and flue gas. This is resulted from the reduced cross sectional area with the larger angle α which promotes the mean velocity in the upstream furnace. Also larger $\overset{*}{K}_v$ is observed in x = 2000 plane than x = 1000 mm plane with the same furnace shape. According to Eq. (4), it can be seen that K_v is in direct proportion to the product of mean density, velocity and area of the upward flow. However, the variance of mean density is negligible compared to that of mean velocity, and the occupation ratio of the upward flow is found to decrease as angle α increases according to Fig. 6b–c (normalized by the reference case). Hence, it implies that the increase of mean velocity is the dominant factor on the strengthened internal recirculation. It further confirms that when designing a furnace under MILD operation, a larger angle α would be helpful for establishing MILD combustion.

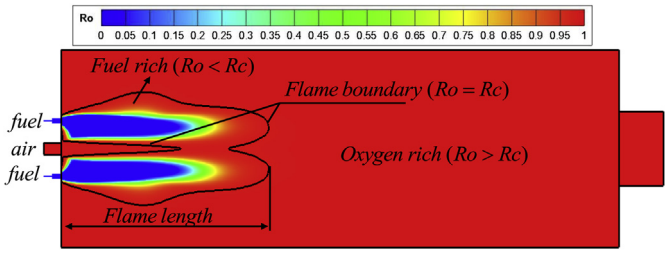

Fig. 11. Schematic diagram of chemical flame.

3.4. Effects of furnace chamber shape on combustion

The uniform temperature distribution has impelled the application of MILD combustion in the industrial heating. The intuitive way to inspect the uniformity of the temperature distribution is to obtain the temperature field inside the furnace directly. According to the experiments [11], the combustion temperature peak did not exceed 1550 °C (1823 K), and the whole furnace was filled with combustion products with temperature in the range of 1300–1500 °C (1573–1773 K). Fig. 9 displays the temperature fields in the x–y plane (z = 0) for the five cases. The isotherms of 1600 K, 1700 K and 1800 K are depicted in the temperature fields. A black arrowed line is also given to represent the variation trend of the area with temperature above 1600 K. It can be found that, with the expansion of angle α, the axial distance of the isotherm of 1600 K reaches further. Moreover, the maximum gas temperature inside the furnace is shown in Fig. 10 for the five cases, and the temperature peak is observed to reduce with the increase of angle α. In this regard, it can be known that the temperature gradient is lower and the temperature uniformity improves as angle α increases.

In the IFRF's experiments, there were no visible flames being observed when natural gas was fired [11], thus, the conventional identification of the flame size with naked eye is no longer applicative to describe MILD combustion. In some sense, MILD combustion is more like the "diffusive combustion" or "volumetric combustion", and the chemical reaction of the combustion reactants takes place in a broader space than conventional combustion. In order to identify the volume of reaction zone, a concept of chemical flame [15,16] is introduced in the present work. It is

described by means of the oxidation mixture ratio (Ro), which is expressed as:

$$R_o = \frac{m_O}{m_O + m'_O} \tag{6}$$

where m_O is the local mass fraction of oxygen, and m'_O is the total mass fraction of oxygen needed to complete combustion. In the present study, the combustible species contains CH_4, C_2H_6, C_3H_8, CO, H_2. To complete the combustion, the needed oxygen amount (m'_O) is calculated as:

$$m'_O = (2Y_{CH_4} + 3.5Y_{C_2H_6} + 5Y_{C_3H_8} + 0.5Y_{CO} + 0.5Y_{H_2})M_{O_2} \tag{7}$$

where Y_i is the volume fraction of the combustible species, and M_{O2} is the molecular mass of oxygen. Thus, Eq. (6) can be transformed as:

$$R_o = \frac{Y_{O_2}M_{O_2}}{Y_{O_2}M_{O_2} + (2Y_{CH_4} + 3.5Y_{C_2H_6} + 5Y_{C_3H_8} + 0.5Y_{CO} + 0.5Y_{H_2})M_{O_2}} = \frac{Y_{O_2}}{Y_{O_2} + 2Y_{CH_4} + 3.5Y_{C_2H_6} + 5Y_{C_3H_8} + 0.5Y_{CO} + 0.5Y_{H_2}} \tag{8}$$

For fuel and oxidizer inlet, the value of R_O is 0 and 1, respectively. $R_O = Rc$ is assumed to indicate the flame boundary, and chemical flame is assumed to be inside the space where $0 < R_O \leq Rc$ as shown in Fig. 11. Note that, it does not mean that there is actual flame inside the chemical flame boundary, since the aim of introducing this concept is to describe the reaction zone semi quantitatively. In order to validate the exact value for Rc, experimental and simulation work has been carried out by Yang et al. [15] and Li et al. [16], and the value of 0.99 was found to be adequate to describe the flame size. Therefore, $Rc = 0.99$ is also adopted in this paper to represent the chemical flame border.

Fig. 12 displays the contours of chemical flame shape in the x-y plane ($z = 0$) and the y-z planes at $x = 1000$ mm and 2000 mm for the five cases. The chemical flame border is represented by a black curve. Similar flame pattern is observed with a double parallel peak shape for each case. According to Fig. 12a, a slight increase of the chemical flame length (the axial maximum distance of the chemical flame boundary) is observed as angle α increases. Simultaneously, the occupation ratio of chemical flame in both $x = 1000$ mm and $x = 2000$ mm planes (normalized by the reference case) is found to be enlarged with the increase of angle α (see Fig. 12b–c).

In order to specify the characteristic of volumetric combustion under MILD condition, chemical flame occupation degree (R_F) is introduced here, which is defined as the ratio between the chemical flame volume (V_f) and the furnace volume (V_F), and is calculated as:

$$R_F = \frac{V_f}{V_F} \tag{9}$$

According to the calculated R_F for the five cases (see Fig. 13), R_F increases with angle α, which means that the chemical flame volume expands as the angle α increases. This is caused by the improved mean velocity and strengthened internal recirculation under larger angle α. Consequently, the dilution of the reactants is facilitated, and the chemical reaction slows down. All the above observations of combustion temperature and chemical flame indicate that, the larger angle α would lead to a larger reaction zone as well as slower reaction rate, if more uniform temperature is required, angle α is suggested to be larger.

3.5. Effects of furnace chamber shape on NO_x emission

During the combustion of natural gas under air condition, there are two major NO formation mechanisms, namely the thermal-NO and the prompt-NO. Thermal-NO is formed by the oxidation of molecular nitrogen, and is favored under high temperature condition [44]. Prompt-NO is formed by the oxidation of nitrogen radicals especially under fuel-rich condition [45]. Besides, NO can be reduced by the intermediate species like CH_i radicals, and subsequently changes to HCN, which is known as the NO-reburning mechanism [46]. However, HCN can be further oxidized to NO. In the present simulations, NO was calculated using the post-processing method considering the thermal, prompt and the reburning mechanisms.

Table 4 reports the predicted NO emission for the five calculated cases. Note that, the high temperature oxidizer contains as high as 110 ppm NO which takes up a large part of the total NO emission. According to Table 4, the net NO formation reduces when increasing the angle α. This may be resulted from two reasons: First, the reduced temperature restrains the formation of thermal-NO since the thermal-NO is quite sensitive to the combustion temperature. Second, the stronger internal recirculation enhances the dilution degree of the reactants. Hence, a more reductive atmosphere can even be created which promotes the NO-reburning mechanism. Furthermore, the promoted reductive atmosphere seems to be helpful for the prompt-NO generation. However, it is found that the amount of prompt-NO is comparable to that of reburning-NO. Consequently, the contribution to the NO reduction mainly comes from the reduction of thermal-NO.

4. Conclusion

This study numerically investigated the effects of furnace chamber shape on natural gas in an industrial-scale furnace under MILD operation. The furnace chamber shape is varied by changing the angle α between the furnace roof and sidewall from 80° to 100°. The prediction with the adopted models for the reference case shows good agreement with the experimental results, and the conclusions are as follows:

In the present furnace-burner system, the furnace chamber shape has a significant impact on in-furnace mixing and combustion characteristics. Increasing angle α would cause a stronger recirculation flow field with more combustion products entrained into the reactants. This results in a broader reaction zone and further leads to a lower combustion temperature peak and NO_x emission.

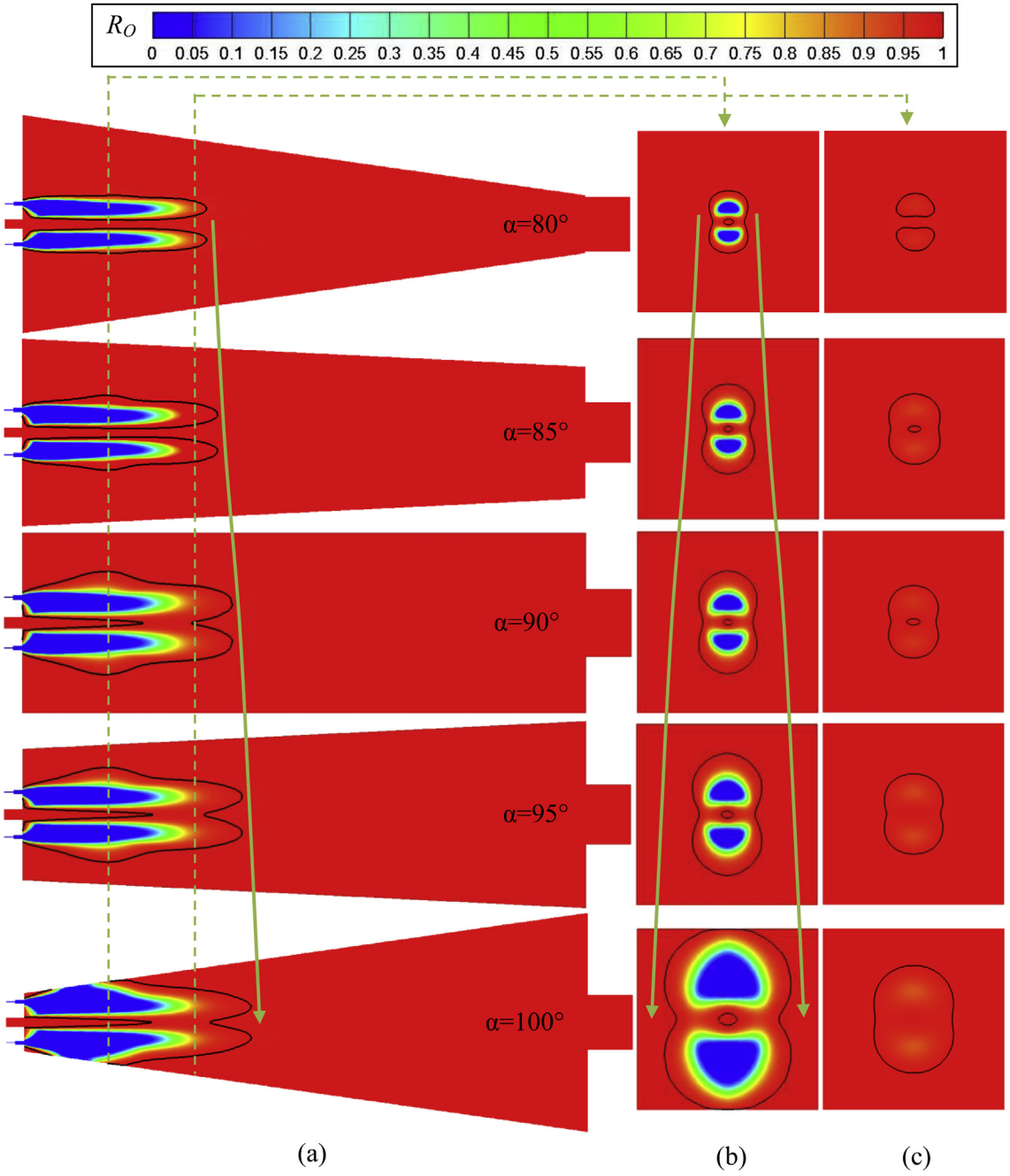

Fig. 12. Contours of chemical flame shape (a): x–y plane ($z = 0$); (b): $x = 1000$ mm; (c): $x = 2000$ mm. The black curves denote the level of Ro = 0.99.

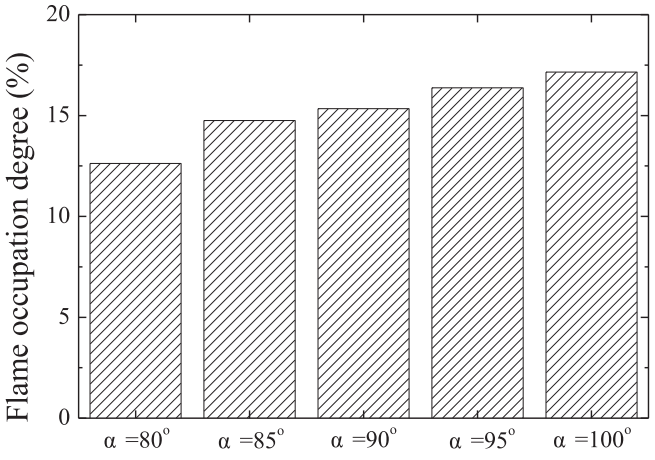

Fig. 13. Chemical flame occupation degree for the five cases.

Table 4
Predicted NO_x in the flue gas for the considered cases (unit: ppm, dry).

	Case1	Case2	Case3	Case4	Case5
α	80°	85°	90°	95°	100°
Total-NO*	145	140	131	126	123
Net-NO	35	30	21	16	13
Thermal-NO	142	138	129	125	121
Prompt-NO	6	6	6	7	10
Reburning-NO	3	4	4	6	8

* The Total-NO is calculated by activating both the thermal-NO, prompt-NO and reburning submodels. While Thermal-NO and Prompt-NO are calculated separately.

According to the stability limits of diffusion combustion provided by Wünning et al. [4], the MILD combustion stability in the investigated domain is found to be enhanced when increasing angle α, and this indicates that a relatively large angle α is helpful for establishing MILD combustion under the present conditions. In contrast, the combustion regime becomes unsteady when angle α is less than 85°, and this further implies that the angle α cannot be too small to establish MILD combustion under the present conditions, or the initial injection conditions must be intensified enough.

Acknowledgements

The authors greatfully acknowledge the support of the National Nature Science Foundation of China (Grant 51276074), State Key Development Program for Basic Research of China (Grant 2011CB707301) and Innovation Research Foundation of Huazhong University of Science and Technology (Grant 2014NY008).

References

[1] A. Cavaliere, M.D. Joannon, Mild combustion, Prog. Energy Combust. Sci. 30 (2004) 329–366.
[2] M. Katsuki, T. Hasegawa, The science and technology of combustion in highly preheated air, Proc. Combust. Inst. 27 (1998) 3135–3146.
[3] H. Tsuji, A.K. Gupta, T. Hasegawa, M. Katsuki, K. Kishimoto, M. Morita, High Temperature Air Combustion-from Energy Conservation to Pollution Reduction, CRC Press, 2003.
[4] J.A. Wünning, J.G. Wünning, Flameless oxidation to reduce thermal NO-formation, Prog. Energy Combust. Sci. 23 (1997) 81–94.
[5] J.G. Wünning, Flameless oxidation, in: Proceedings of the 6th High Temperature Air and Gasification Conference (HiTACG). Essen, Germany, 2005.
[6] V.K. Arghode, A.K. Gupta, Effect of flow field for colorless combustion (CDC) for gas turbine combustion, Appl. Energy 87 (2010) 1631–1640.
[7] V.K. Arghode, A.K. Gupta, K.M. Bryden, High intensity colorless distributed combustion for ultra low emission and enhanced performance, Appl. Energy 92 (2012) 822–830.
[8] S. Orsino, M. Tamura, P. Stabat, S. Costantini, O. Prado, R. Weber, Excess Enthalpy Combustion of Coal, Tech. Rep. F46/y/3, IFRF Research Station, 2004.
[9] S. Orsino, R. Weber, Numerical simulation of combustion of natural gas with high-temperature air, Combust. Sci. Technol. 170 (2001) 1–34.
[10] M. Mancini, R. Weber, U. Bollettini, Predicting NO_x emissions of a burner operated in flameless oxidation mode, Proc. Combust. Inst. 29 (2002) 1155–1163.
[11] R. Weber, J. Smart, W. Kamp, On the (MILD) combustion of gaseous, liquid,and solid fuels in high temperature preheated air, Proc. Combust. Inst. 30 (2005) 2623–2629.
[12] N. Schaffel-Mancini, M. Mancini, A. Szlek, R. Weber, Mathematical modeling of MILD combustion of pulverized coal, Combust. Flame 156 (2009) 1771–1784.
[13] N. Schaffel-Mancini, M. Mancini, A. Szlek, R. Weber, Novel conceptual design of a supercritical pulverized coal boiler utilizing high temperature air combustion (HTAC) technology, Energy 35 (2010) 2752–2760.
[14] W. Blasiak, W. Yang, K. Narayanan, J.V. Schéele, Flameless oxyfuel combustion for fuel consumption and nitrogen oxides emissions reductions and productivity increase, J. Energy Inst. 80 (2007) 3–11.
[15] W. Yang, W. Blasiak, Numerical study of fuel temperature influence on single gas jet combustion in highly preheated and oxygen deficient air, Energy 30 (2005) 385–398.
[16] J. Li, E. Biagini, W. Yang, L. Tognotti, W. Blasiak, Flame characteristics of pulverized torrefied-biomass combusted with high-temperature air, Combust. Flame 160 (2013) 2585–2594.
[17] G.G. Szegö, B.B. Dally, G.J. Nathan, Operational characteristics of a parallel jet MILD combustion burner system, Combust. Flame 156 (2009) 429–438.
[18] B.B. Dally, S.H. Shim, R.A. Craig, P.J. Ashman, G.G. Szegö, On the burning of sawdust in a MILD combustion furnace, Energy Fuels 24 (2010) 3462–3470.
[19] J. Mi, P. Li, C. Zheng, Impact of injection conditions on flame characteristics from a parallel multi-jet burner, Energy 36 (2011) 6583–6595.
[20] J. Mi, F. Wang, P. Li, B.B. Dally, Modified vitiation in a moderate or intense low-oxygen dilution (MILD) combustion furnace, Energy Fuels 26 (2012) 265–277.
[21] P. Li, J. Mi, B.B. Dally, R.A. Craig, F. Wang, Premixed moderate or intense low-oxygen dilution (MILD) combustion from a single jet burner in a laboratory-scale furnace, Energy Fuels 25 (2011) 2782–2793.
[22] J. Mi, P. Li, B.B. Dally, R.A. Craig, Importance of initial momentum rate and air-fuel premixing on moderate or intense low oxygen dilution (MILD) combustion in a recuperative furnace, Energy Fuels 23 (2009) 5349–5356.
[23] S. Chen, J. Mi, H. Liu, C. Zheng, First and second thermodynamic-law analyses of hydrogen-air counter-flow diffusion combustion in various combustion modes, Int. J. Hydrogen Energy 37 (2012) 5234–5245.
[24] M. Vascellari, G. Cau, Influence of turbulence–chemical interaction on CFD pulverized coal MILD combustion modeling, Fuel 101 (2012) 90–101.
[25] T. Suda, M. Takafuji, T. Hirata, M. Yoshino, J. Sato, A study of combustion behavior of pulverized coal in high temperature air, Proc. Combust. Inst. 29 (2002) 503–509.
[26] R. He, T. Suda, M. Takafujil, T. Hirata, J. Sato, Analysis of low NO emission in high temperature air combustion for pulverized coal, Fuel 83 (2004) 1133–1141.
[27] D. Ristic, A. Schuster, G. Scheffknecht, H. Stadler, M. Förster, R. Kneer, Experimental study on flameless oxidation of pulverized coal in bench and pilot scale, in: Proceedings of the 23th German Flameday. Berlin, Germany, 2007.
[28] D. Ristic, M. Schneider, A. Schuster, G. Scheffknecht, J. Wünning, Investigation of NOX formation for flameless coal combustion, in: 7th High Temperature Air Combustion and Gasification International Symposium. Phuket, Thailand, 2008.
[29] H. Stadler, D. Ristic, M. Förster, A. Schuster, R. Kneer, G. Scheffknecht, NOX-emissions from flameless coal combustion in air, Ar_O2 and CO2_O2, Proc. Combust. Inst. 32 (2009) 3131–3138.
[30] H. Stadler, D. Toporov, M. Förster, R. Kneer, On the influence of the char gasification reactions on NO formation in flameless coal combustion, Combust. Flame 156 (2009) 1755–1763.
[31] H. Stadler, Experimental and Numerical Investigation of Flameless Pulverized Coal Combustion, Ph.D. Thesis, the University of Adelaide, Adelaide, South Australia, 2010.
[32] H. Stadler, D. Christ, M. Habermehl, P. Heil, A. Kellermann, A. Ohliger, D. Toporov, R. Kneer, Experimental investigation of NOX emissions in oxycoal combustion, Fuel 90 (2011) 1604–1611.
[33] H. Zhang, G. Yue, J. Lu, Z. Jia, J. Mao, T. Fujimori, T. Suko, T. Kiga, Development of high temperature air combustion technology in pulverized fossil fuel fired boilers, Proc. Combust. Inst. 31 (2007) 2779–2785.
[34] C. Tang, M. Fang, Z. Tang, Q. Lin, Experimental study on the oxy-fuel flameless combustion of pulverized coal, Power Syst. Eng. 26 (2010) 8–10 (in Chinese).
[35] Y. Tu, H. Liu, R. Zhao, Z. Liu, J. Mi, C. Zheng, Numerical calculation of MILD combustion for pulverized coal on 0.3MW furnace, J. Combust. Sci. Technol. 19 (2013) 444–451 (in Chinese).
[36] Y. Tu, H. Liu, P. Li, F. Wang, T. Zhang, C. Bai, Y. Zheng, Z. Liu, J. Mi, C. Zheng, Experimental study of MILD combustion for pulverized coal in 0.3MW vertical furnace, in: 9th Asia-Pacific Conference on Combustion, Gyeongju, Korea, 2013.
[37] B. Danon, E.S. Cho, W. de Jong, D. Roekaerts, Numerical investigation of burner positioning effects in a multi-burner flameless combustion furnace, Appl. Therm. Eng. 31 (2011) 3885–3896.
[38] B. Danon, E.S. Cho, W. de Jong, D. Roekaerts, Parametric optimization study of a multi-burner flameless combustion furnace, Appl. Therm. Eng. 31 (2011) 3000–3008.

[39] B.E. Launder, D.B. Spalding, The numerical computation of turbulent flows, Comput. Meth. Appl. Mech. Eng. 3 (1974) 269–289.
[40] P. Cheng, Two-dimensional radiating gas flow by a moment method, AIAA J. 2 (1964) 1662–1664.
[41] S. Patankar, D. Spalding, A calculation procedure for heat, mass and momentum transfer in three-dimensional parabolic flows, Int. J. Heat Mass Transf. 15 (1972) 1787–1806.
[42] C. Galletti, A. Parente, L. Tognotti, Numerical and experimental investigation of a mild combustion burner, Combust. Flame 151 (2007) 649–664.
[43] G.Q. Smith, D.M. Golden, M. Frenklach, N.W. Moriarty, B. Eiteneer, M. Goldenberg, et al. http://www.me.berkeley.edu/gri_mech/.
[44] Y.B. Zeldovich, P.Y. Sadovnikov, D.A. Frank-Kamenetskii, Oxidation of Nitrogen in Combustion, Publishing House of the Academy of Sciences, Moscow-Leningrad, USSR, 1947.
[45] C. Fenimore, Formation of nitric oxide in premixed hydrocarbon flames, Proc. Combust. Inst. 13 (1971) 373–380.
[46] W. Chen, L. Smoot, S. Hill, T. Fletcher, Global rate expression for nitric oxide reburning, Part 2, Energy Fuels 10 (1996) 1046–1052.